Anisotropic Self-Diffusion in Block Copolymer Cylinders

Kevin A. Cavicchi and Timothy P. Lodge*,†

Department of Chemical Engineering and Materials Science, University of Minnesota, Minneapolis, Minnesota 55455

Received March 8, 2004; Revised Manuscript Received May 31, 2004

ABSTRACT: Self-diffusion measurements have been performed on an ordered asymmetric poly(ethylene-*alt*-propylene-*b*-dimethylsiloxane) PEP−PDMS block copolymer (M_n = 30 000, f_{PEP} = 0.79) using forced Rayleigh scattering (FRS). Samples were prepared with three different degrees of macroscopic alignment of the hexagonally packed PDMS cylinders. The diffusion coefficients parallel (D_{par}) and perpendicular (D_{perp}) to the cylinder axes were resolved. For a high degree of macroscopic alignment both D_{par} and D_{perp} were found to be significantly retarded compared to D_0, the diffusion coefficient in the absence of any interactions. D_{perp} follows a hindered diffusion mechanism, while D_{par} is consistent with a block retraction mechanism; both of these mechanisms have been described previously in the context of block copolymer spheres and lamellae, respectively. The extracted D_{perp} was dependent on the degree of alignment, with the apparent D_{perp} increasing as the degree of alignment deteriorated, whereas D_{par} was essentially independent of the degree of alignment. This behavior of D_{perp} is interpreted in terms of defects in the samples (i.e., both misoriented cylinders and dislocations).

Introduction

In ordered block copolymers the thermodynamic potential field experienced by individual chains can retard self-diffusion because there is an enthalpic penalty to mixing the two blocks. The extent of retardation and the mechanisms of diffusion are dependent on various factors including the particular microphase, the chain length, the degree of entanglement, and the immiscibility between the blocks. Retarded diffusion has been observed in lamellar,[1−8] hexagonal cylinder,[6,7,9−12] gyroid,[11,13] and body-centered-cubic (bcc) sphere phases.[6,13−15]

In lamellar and cylinder samples two diffusion coefficients can be defined: D_{par}, for diffusion along the interface, and D_{perp}, for diffusion across the interface. In contrast, in bcc spheres only one diffusion coefficient, D_s, is needed because the chains diffuse isotropically, by hopping from sphere to sphere. To a good approximation D_s and D_{perp} should be equivalent, and indeed both D_s and D_{perp} (in both lamellae and cylinders) have been found to follow a hindered diffusion mechanism, with D given by[5,9,14,16,17]

$$D \sim D_0 \exp(-\alpha\chi N_A) \quad (1)$$

where χ is the Flory−Huggins interaction parameter and N_A is the degree of polymerization of the block being pulled into the unfavorable domain. D_0 is the diffusion coefficient in the absence of any interactions (i.e., as $\chi \rightarrow 0$), and α is a parameter on the order of unity, but which experimentally depends on χN. In the hexagonal cylinder and sphere phases N_A refers to the core block, whereas in the lamellar phase N_A refers to the longer block.

The behavior of D_{par} is more complicated. The mechanism of diffusion depends on both the degree of entanglement and the degree of segregation in the system. In unentangled systems, $D_{par} \approx D_0$ because a chain can diffuse freely along the interface without mixing the two blocks.[10,18] In an entangled system the average tube for a given chain will lie perpendicular to the interface, and therefore the chain cannot diffuse readily along the interface as it did in an unentangled system.[19] In poly(ethylene-*alt*-propylene-*b*-ethylethylene) (PEP−PEE) lamellae and cylinders, where both blocks were above their entanglement molecular weights, D_{par} was found to follow a hindered diffusion mechanism analogous to eq 1.[5,6] In this case the reptation process forces mixing of the two blocks, whether the chain is moving parallel or perpendicular to the interface. However, for tracers in a high molecular weight PEP−PEE lamellar matrix, the normalized diffusion coefficient, D_{par}/D_0, was found to be independent of temperature (and thus χ) but dependent on the molecular weight of the tracer.[5] A new mechanism of diffusion, block retraction, was proposed.[20] Instead of the chain reptating across the interface, the blocks retract to the interface and then reinsert themselves into their respective domains, in a manner similar to the arm retraction mechanism for diffusion of entangled branched homopolymers.[21,22] In this case, the diffusion barrier depends on the chain length of the more entangled block:

$$D_{par} = D_0 \exp(-\xi\gamma N_B/N_e) \quad (2)$$

where N_B is the degree of polymerization of the more entangled block, N_e is the corresponding entanglement length, γ is the fraction of the B block that extends beyond the interface into the region of pure B, and ξ is a constant of order unity. This mechanism has not yet been reported in cylinders.

The different mechanisms of diffusion for D_{par} and D_{perp} result in anisotropic diffusion. In unentangled polymers, as χ is increased, D_{perp} will become more retarded compared to D_0 and D_{par}, and therefore the anisotropy of diffusion, D_{par}/D_{perp}, will increase exponentially as χ increases. Hamersky et al. have resolved D_{par}/D_{perp} values as large as 40 in poly(styrene-*b*-isoprene) lamellae[10] for $\chi N_A \approx 10$ and ca. 80 in poly-

† Also Department of Chemistry, University of Minnesota, Minneapolis, MN 55455.
* Author for correspondence: e-mail lodge@chem.umn.edu.

10.1021/ma0495339 CCC: $27.50
Published on Web 07/10/2004

(ethylene oxide-*b*-ethylethylene) cylinders[11] for $\chi N_A \approx 8$. Rittig et al. reported an anisotropy of diffusion of 60 in poly(ethylene-*alt*-propylene-*b*-dimethylsiloxane) (PEP−PDMS) cylinders[9] at $\chi N_A \approx 9$.

In entangled block copolymers, when both D_{par} and D_{perp} follow the hindered diffusion mechanism, the anisotropy of diffusion should be reduced. In PEP−PEE cylinders, no appreciable anisotropy was detected as $D_{par} \approx D_{perp}$ ($4.75 < \chi N_A < 6$).[6] In a PEP−PEE lamellar sample D_{par}/D_{perp} ranged from 1 to 3 ($12 < \chi N_A < 15$).[23] A small anisotropy could result from slightly different dependences of D_{par} and D_{perp} on χN_A. On the other hand, a larger anisotropy is expected when D_{par} follows a block retraction mechanism, as D_{par} will be independent of χ while D_{perp} will still be strongly dependent on χ.

Measurements of D_{par} and D_{perp} are facilitated by macroscopically aligned samples. (One exception to this was the pulsed field gradient NMR study of Rittig et al. on PEP−PDMS cylinders.[9] Although the sample was unaligned, the experimental signals were deconvoluted into the contributions from D_{par} and D_{perp}.) However, it is difficult to achieve a perfect, macroscopic "single crystal" block copolymer sample. Thus, defects in the alignment can affect the measurement of D_{par} and D_{perp}. For example, in forced Rayleigh scattering (FRS) measurements by Hamersky et al. on PEO−PEE cylinders two modes of diffusion were observed.[11] They were interpreted as either parallel or perpendicular diffusion in well-aligned regions, depending on the orientation of the sample, and diffusion in regions with a high amount of defects. The diffusion coefficient in the defective regions was intermediate between D_{par} and D_{perp}, reflecting a local averaging of the two diffusion coefficients.

In this report we present FRS diffusion measurements on a PEP−PDMS polymer in the hexagonal cylinder phase, with PDMS cylinders in a PEP matrix. FRS measures the diffusion coefficient along one selectable direction, so macroscopically aligned cylinder samples can be oriented to measure both D_{par} and D_{perp}. In contrast to previous measurements on cylinders, which measured diffusion on an unaligned sample and one aligned sample,[11] samples with three different degrees of alignment were examined. In addition, comparisons are made to recent measurements of the tracer diffusion of the same polymer in a bcc sphere matrix.[14] The resulting values of D_{par} are consistent with a crossover from hindered reptation to block retraction with increasing χN_A, and the measured values were rather insensitive to the degree of alignment. This is the first observation of block retraction in the hexagonal cylinder phase. In contrast, D_{perp} is consistent with a hindered diffusion process, but with substantial sensitivity to the degree of alignment. The differing sensitivities of D_{par} and D_{perp} to the degree of alignment are due to the role defects play in providing a faster route to diffusion than perpendicular diffusion.

Experimental Section

Materials. Diffusion measurements were made on an asymmetric poly(ethylene-*alt*-propylene-*b*-dimethylsiloxane) (PEP−PDMS) block copolymer ($M_n = 30\,000$, $f_{PEP} = 0.79$, $N_{PEP} = 340$, $N_{PDMS} = 91$). The interaction parameter for this system is $\chi = 64\ \mathrm{K}/T - 0.03$[24] based on the T_{ODT} of two lamellar PEP−PDMS polymers and the predicted $(\chi N)_{ODT}$ from the theory of Fredrickson and Helfand.[25] The details of the polymerization and labeling of this polymer for diffusion measurements have been presented previously.[14] The photochromic dye 4′-(*N*,*N*-dimethylamino)-2-nitrostilbene-4-carboxylic acid was attached to a fraction of the copolymer chains by reaction with terminal hydroxyl groups. The PEP and PDMS block lengths were determined using a common reference volume obtained from the geometric mean of the monomer molar volumes.

Forced Rayleigh Scattering (FRS). The experimental details have been presented previously.[23,26] Samples were prepared using 5 wt % labeled polymer. The labeled and unlabeled polymer were dissolved in methylene chloride, filtered through an 0.45 μm PTFE filter, precipitated in methanol, and dried to constant weight under vacuum. FRS samples were prepared by three different methods to achieve different degrees of macroscopic alignment. For method one, the polymer was pressed into a ca. 1 mm thick strip using a channel die and a portion was cut out using a circular punch and placed in an FRS sample cell consisting of two circular glass slides separated by a 1 mm aluminum spacer. The channel consisted of a U-shaped metal block with a 6 mm × 60 mm channel and a separate plunger with the same dimensions. Teflon strips were glued to both the bottom of the channel and the plunger prior to pressing. For method two, a 1 mm aluminum spacer was glued to a circular glass slide. A volume of polymer greater than that needed to fill the spacer was placed inside the spacer. The polymer was pressed to fill the spacer using a second glass slide. The excess polymer was removed, and the sample was sealed. In method three, 500 mg of polymer was pressed using a 25 mm diameter cylindrical die to ca. 1 mm thickness. The die consisted of an aluminum cylinder with a 25 mm diameter hole bored through the center and an accompanying plunger. A portion was cut out with a circular punch and placed in an FRS sample cell. The fitting of the FRS intensity decays will be discussed subsequently.

Small-Angle X-ray Scattering (SAXS). SAXS measurements were made using the 6 m SAXS line at the University of Minnesota. X-rays were generated using a rotating anode (Rigaku RU-200BVH) with a pin-focus cathode and Franks mirror optics. 2-D patterns were recorded on a multiwire detector (Siemens), with a sample-to-detector distance of 3.2 m. The sample chamber was an in-line parallel plate rheometer (Rheometrics DMTA). The sample was mounted on the plate so the beam was in the same direction as the force used to press the samples. The degree of alignment of the cylinders was quantified using the second-order orientation factor, F_2.[27−30] The intensity was integrated as a function of the azimuthal angle, θ, in a ring about the principal peak wavevector q^*, with a width given by the full width at half-maximum of the primary peak, resulting in the scattered intensity as a function of angle, $I(q^*,\theta)$ ($\theta = 90°$ at the peak in intensity). The normalized orientation distribution function of the cylinder axes is

$$P(\beta) = \frac{I(q^*,\theta)q^{*2}}{\int_0^{\pi} I(q^*,\theta)q^{*2} \sin\theta\, \mathrm{d}\theta} \tag{3}$$

The second-order orientation parameter is given as

$$F_2 = 1 - 3\langle \cos^2\theta \rangle \tag{4}$$

where $\langle \cos^2\theta \rangle$ is

$$\langle \cos^2\theta \rangle = \int_0^{\pi} \cos^2\theta P(\theta) \sin\theta\, \mathrm{d}\theta \tag{5}$$

If the cylinders were perfectly aligned, $P(\theta)$ would be a delta function at 90° and $F_2 = 1$. If the alignment is isotropic, $P(\theta)$ is independent of θ and $F_2 = 0$. There is a finite beam size in the experiment, so the highest F_2 value that can be expected experimentally is 0.99.[28]

Static Birefringence. Static birefringence measurements were made with the following optical train. A He−Ne laser beam (633 nm) was passed through a vertical polarizer, a

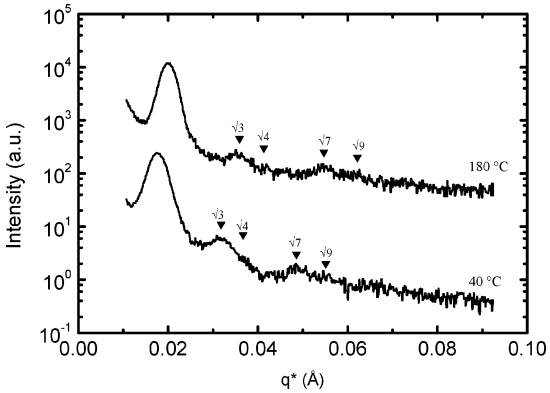

Figure 1. Azimuthally averaged SAXS intensity profiles for EPDMS 23-7 at 40 and 180 °C. The higher order peak positions are indicated on each profile.

quarter-wave plate, the sample, an iris, and a rotatable analyzer. The transmitted intensity was measured by a photodiode as a function of analyzer orientation and reported as a voltage.

Transmission Electron Microscopy (TEM). TEM measurements was made using an electron microscope (JEOL 1210) operating in bright field mode at 120 kV. Images were obtained using a CCD camera. The samples were unstained as the Si in the PDMS block provided sufficient contrast between the two blocks.

Results and Discussion

This section is divided into four parts. Part 1 discusses the phase behavior and the macroscopic alignment of EPDMS 23-7. Part 2 discusses the FRS intensity decay fitting. Parts 3 and 4 discuss the mechanisms of diffusion and the dependence of the diffusion coefficients on the degree of alignment, respectively.

Phase Behavior and Macroscopic Alignment. Figure 1 shows azimuthally averaged SAXS intensity profiles taken at 40 and 180 °C on an unaligned EPDMS 23-7 sample. The allowed q/q^* ratios for the hexagonal cylinder phase are 1, $\sqrt{3}$, $\sqrt{4}$, $\sqrt{7}$, $\sqrt{9}$, ...; the agreement of the peak positions with these ratios confirms that the polymer forms the expected hexagonally packed PDMS cylinders in a PEP matrix.

Table 1. F_2 for Each Sample Preparation Method

preparation method	F_2
channel die press	0.77
press between glass slides	0.26
cylindrical die press	0.07

Figure 2 shows representative 2D SAXS patterns of the samples with the beam along the force (pressing) direction. Each exposure was taken for 900 s. For patterns b and c the actual FRS samples were used, while for pattern a, a sample prepared under identical conditions was used. Also included in Figure 2 are plots of the intensity about the primary peak vs the azimuthal angle, which are used to determine F_2. In each plot a background intensity has been subtracted. Table 1 lists the F_2 value for each sample. In the channel die, the cylinders align along the flow direction, resulting in the highest degree of alignment. In the other samples the flow is radially outward from the center of the sample. The cylinders still align somewhat with the flow, but there is a broader distribution of directions around a preferred cylinder axis orientation.

The FRS experiment measures the diffusion coefficient along one direction. In each sample there is a preferred orientation of the cylinders given by the peak in the intensity vs θ in Figure 2. An orientation angle, ϕ, can be defined describing the preferred orientation of the cylinders with respect to the FRS measurement axis. In this way $\phi = 90°$ corresponds to the perpendicular orientation, and $\phi = 0°$ is the parallel orientation. For each sample D_{perp} and D_{par} refer to the diffusion coefficients measured at $\phi = 90°$ and $\phi = 0°$, respectively.

Static birefringence measurements were made to verify the orientation in each sample after it was sealed. Figure 3 shows a plot of the transmitted intensity vs φ, the angle between the vertical polarization and the analyzer, with the preferred cylinder axis orientation lying in the same direction as the vertical polarization.

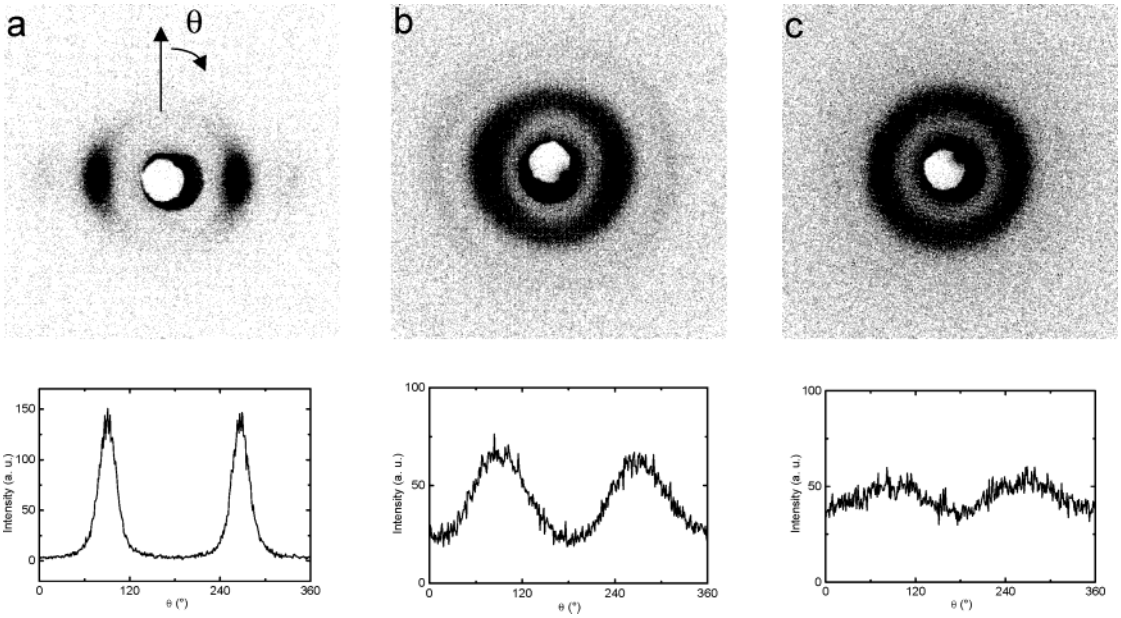

Figure 2. 2-D SAXS patterns for samples prepared with (a) a channel die, (b) glass slides, and (c) a cylindrical die. The intensity vs angle at q^* used for F_2 determination is shown below each pattern.

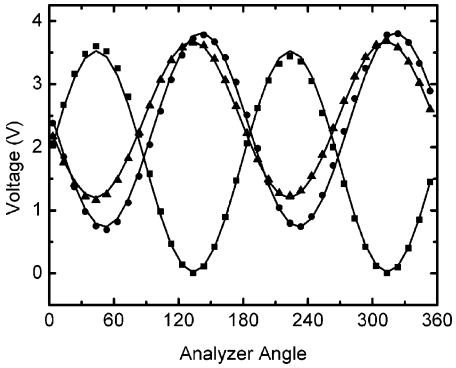

Figure 3. Transmitted intensity vs orientation angle in static birefringence experiment for (■) $F_2 = 0.77$, (●) $F_2 = 0.26$, and (▲) $F_2 = 0.07$. The solid lines are fits to eq 6.

Table 2. I_0, ϕ_p, and δ for Each Sample

F_2	I_0	ϕ_p (deg)	δ (rad)	$\Delta n/\Delta n_0$
0.77	3.54	−2	4.56	1.05
0.26	4.55	6	0.73	0.17
0.07	4.88	−1	0.52	0.12

For aligned cylinders the intensity should vary with angle as[31]

$$I = \frac{I_0}{2}[1 + \sin(2(\varphi - \phi_a))\sin(\delta)] \qquad (6)$$

where I_0 is the incident intensity, δ is the retardance, and ϕ_a is the orientation angle of the sample. (ϕ_a should be a multiple of 90° if the cylinders lie either parallel or perpendicular to the vertical polarization.) The retardance is related to the birefringence, Δn, by

$$\delta = \frac{2\pi L}{\lambda}\Delta n \qquad (7)$$

where λ is the wavelength of the laser and L is the thickness of the sample. The solid curves in Figure 3 are fits to eq 6, and Table 2 contains the resulting I_0, ϕ_a, and δ. For the fits it was assumed that ϕ_a was near 90°. Therefore, the "misalignment angle" is $\phi_a = 90° - \phi_p$. The degree of misalignment in the samples was small, with the largest being 6° for $F_2 = 0.26$. The effect of a misaligned sample on the diffusion measurements will be discussed subsequently. The retardances increase with increasing F_2 as expected, and there is a large difference in δ between sample 1 and samples 2 and 3. This can be seen in Figure 3 because the intensity curve for sample 1 is opposite in sign from that of sample 2 and 3, meaning that δ must be at least π radians greater going from sample 2 to sample 1.

The birefringence of each sample was determined using eq 7 and was compared to the theoretical birefringence, Δn_0, for a perfectly aligned sample. The theoretical birefringence was calculated using the expressions derived previously by Lodge and Fredrickson for the intrinsic and form birefringence of block copolymer cylinders.[32] The theoretical birefringence was estimated to be 4.4×10^{-4}. An alternate order parameter can be defined by $\Delta n/\Delta n_0$, where Δn is the measured birefringence in the sample. Table 2 lists $\Delta n/\Delta n_0$ for each sample. For the channel die aligned sample $\Delta n/\Delta n_0$ is actually slightly larger than unity, which indicates a highly aligned sample given the uncertainties inherent in the analysis. The other two samples have a much lower $\Delta n/\Delta n_0$, indicating they are not as well aligned, in agreement with the SAXS results. On the whole we suspect the SAXS-derived order parameters are more quantitatively reliable, as they do not rely on theoretical estimates.

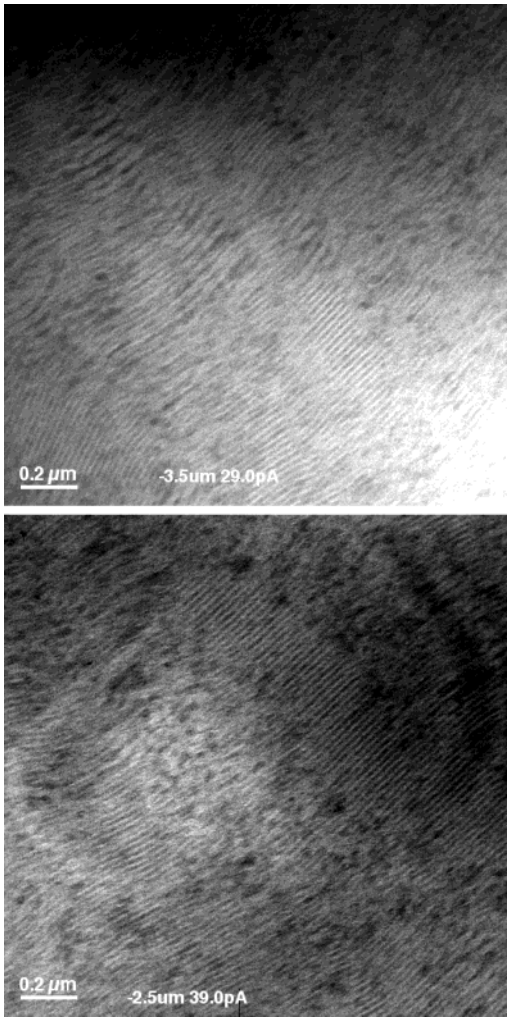

Figure 4. TEM images of the sample pressed in the channel die. The beam is in the same direction as the force used to press the sample.

TEM was used to examine the sample aligned in the channel die. Figure 4 shows images taken with the beam in the force direction, showing the cylinders running through the sample. The cylinders contain Si atoms and therefore appear darker than the matrix in the bright field image. There is clearly a preferred orientation, but the alignment is not perfect as there is some "waviness" to the cylinders.

FRS Signal Analysis. Figure 5a shows FRS intensity decays measured for the sample with $F_2 = 0.77$ in the perpendicular and parallel orientations, at 100 °C and a grating spacing, d, of 1 μm. A baseline intensity has been subtracted from each decay, and the intensity has been normalized by the maximum intensity for clarity. The relaxation time in the parallel orientation is significantly smaller than in the perpendicular orientation, indicating that there is an anisotropy of motion in the sample. The smooth curves through the points are fits to a stretched exponential function

$$I = [A\exp(-(t/\langle\tau\rangle)^{\beta})]^2 + B \qquad (8)$$

where A is a constant, $\langle\tau\rangle$ is the average relaxation time,

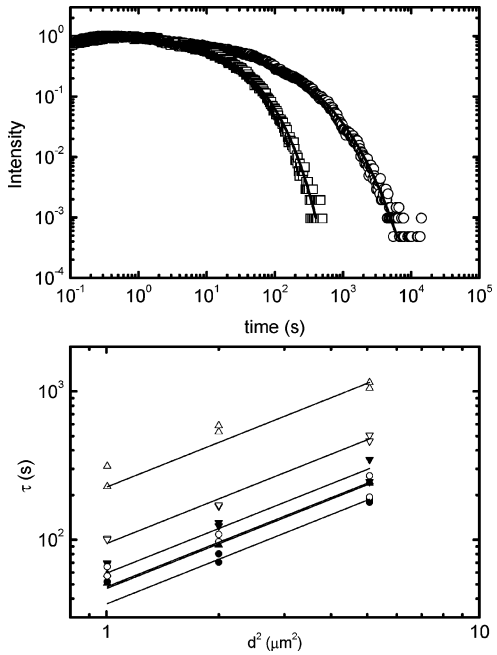

Figure 5. (a) FRS intensity decays for sample 1: (□) parallel orientation, (○) perpendicular orientation. (b) τ vs d^2 for (▲) parallel, $F_2 = 0.77$, (△) perpendicular, $F_2 = 0.77$, (▼) parallel, $F_2 = 0.26$, (▽) perpendicular, $F_2 = 0.26$, (●) parallel, $F_2 = 0.07$, (○) perpendicular, $F_2 = 0.07$.

B is the (incoherent) baseline, and β is related to the width of the distribution of relaxation times. For a single relaxation time, $\beta = 1$. Previously, stretched exponential fits were used for FRS decays of tracer diffusion in sphere-forming block copolymers.[14] The broad distribution of diffusion coefficients was attributed to the polydispersity of the chain lengths, which contributes both through the dependence of D_0 on chain length ($D \sim N^{-2.3}$) and through the dependence on the core block length in the exponential (eq 1). For either the hindered diffusion or block retraction mechanism the chain length appears in the exponential, which will therefore result in a broadened distribution of diffusion coefficients.

For all of the decays in each sample, the fits were begun after $t = 1$ s, ignoring the initial intensity rise. This rise has been attributed to the photoisomerization of the dye and/or thermal relaxation in the sample.[11,33] For the decays at $F_2 = 0.77$, this initial rise was fit by including a second exponential with a relaxation time τ_2 and a negative amplitude, as shown in eq 9.

$$I = (A \exp(-(t/\langle\tau\rangle)^{\beta}) - C \exp(-t/\tau_2))^2 + B \qquad (9)$$

The relaxation times for the intensity rise were independent of the grating spacing, indicating that it is not a diffusive process. Furthermore, the diffusion coefficients obtained from fits using either eq 8 or eq 9, in both the parallel and perpendicular orientations, did not differ by more than 10%. Therefore, the decays at $F_2 = 0.26$ and 0.07 were also fit using eq 8, beginning at $t = 1$ s.

The relaxation time is related to the grating spacing by

$$\tau = \frac{d^2}{4\pi^2 D} \qquad (10)$$

Figure 5b shows plots of τ vs d^2 at $F_2 = 0.77$, 0.26, and 0.07, for both the parallel and perpendicular orientations, at 100 °C. The linearity with a slope of 1 on a log−log scale indicates that the relaxation is due to diffusion. A diffusion coefficient is determined from the slope of a plot of τ vs d^2. A second diffusion coefficient is also determined from a plot of $1/\tau$ vs $1/d^2$. Following standard FRS practice, the reported diffusivities are the arithmetic mean of these two diffusion coefficients to avoid weighting the data at high or low d^2.

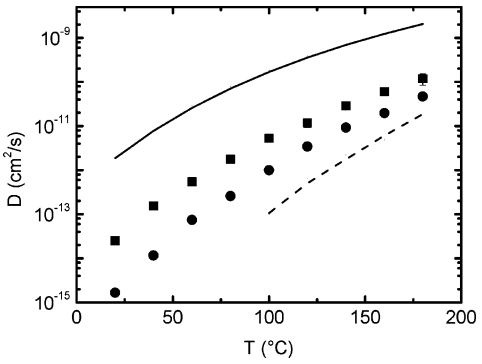

Figure 6. D vs T at $F_2 = 0.77$. (■) D_{par}, (●) D_{perp}, (—) D_0 (- - -) D_s.

From the birefringence measurements, it was determined that at $F_2 = 0.26$ the orientation angle was off by 6° during measurements. The diffusion coefficients at $\phi = 0°$ and $\phi = 90°$ can be estimated using eq 11 and the measured values of $D(\phi)$ at $\phi = -6°$ and $\phi = 84°$.

$$D(\phi) = D_{perp} \sin^2(\phi) + D_{par} \cos^2(\phi) \qquad (11)$$

Equation 11 describes the expected dependence of the diffusion coefficient on the orientation angle where there is anisotropic diffusion.[34] The difference between the measured diffusion coefficients and D_{perp} and D_{par} calculated using eq 11 is less than 1%. At higher degrees of anisotropy a misalignment of the sample would result in a larger error, but even for $F_2 = 0.77$ the departure in D_{par} and D_{perp} from the measured values due to the 2° misalignment is less than 2%.

Diffusion in Aligned Cylinders. Figure 6 shows the diffusion coefficients measured for $F_2 = 0.77$ in the parallel and perpendicular orientations; $D_{par} > D_{perp}$ at all temperatures examined. The error bars (95% confidence interval) were between 5 and 30% and were omitted when they were smaller than the symbol in the plot. These are consistent with the typical uncertainties measured using FRS.[35,36] For comparison, $D_0(T)$ has been shown as a smooth curve. $D_0(T)$ has been estimated from the temperature-dependent diffusivity of a disordered asymmetric PEP−PDMS (EPDMS 11−1, M_n = 12 100, $f_{PEP} = 0.90$). The diffusivity of this polymer was previously shown to be unhindered in the disordered state.[14] D_0 is estimated by scaling the temperature-dependent diffusivity of EPDMS 11-1 to match the molecular weight of EPDMS 23-7 by

$$D_0 = D_{\text{EPDMS 11−1}}(M_{tracer}/M_{\text{EPDMS 11−1}})^{-2.3} \qquad (12)$$

The diffusivity of EPDMS 23-7 as a tracer in a bcc sphere matrix, designated D_s, is also included as a dashed line.[14] D_s should give an estimate of the expected D_{perp} in perfectly aligned cylinders. The three important observations from Figure 6 are that D_{par} and D_{perp} are both retarded compared to D_0, there is a significant anisotropy of diffusion, and D_{perp} is larger than D_s. The

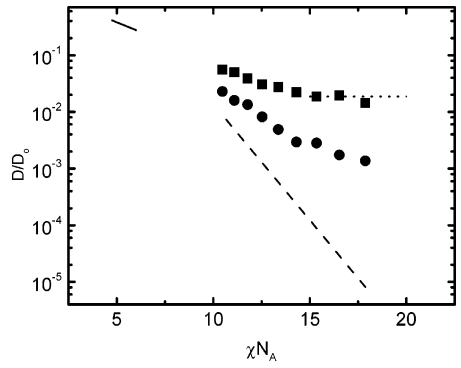

Figure 7. D/D_0 vs χN_A at $F_2 = 0.77$. (■) D_{par}/D_0, (●) D_{perp}/D_0, (—) D/D_0 (PEP−PEE cylinders) (- - -) D_s, (· · ·) block retraction fit.

first two results are consistent with both D_{par} and D_{perp} following a hindered diffusion process at high temperature (small χN_A), but with D_{par} crossing over to the block retraction mechanism at low temperature (larger χN_A). The third result we attribute to the role of defects.

Figure 7 shows a plot of D/D_0 vs χN_A for D_{par} and D_{perp} at $F_2 = 0.77$. The solid line segment at small χN_A is a fit to eq 1 of both D_{par}/D_0 and D_{perp}/D_0 reported previously in PEP−PEE cylinders.[6] The dashed line is a fit of eq 1 to the D_s/D_0 data previously reported in the same system.[14] Clearly D_{perp} lies well above D_s. If D_{perp} and D_{par} both followed a hindered diffusion mechanism, the trajectories of the normalized diffusion coefficients should approach D_s/D_0 with increasing χN_A with α increasing to near unity. This is not the case for D_{par}/D_0, as the dependence on χN_A is much weaker than for either D_{perp} or D_s, and the dependence appears to decrease at the higher χN_A values. As discussed in the Introduction, in lamellar block copolymers a crossover to the χ-independent diffusion mechanism of block retraction has been observed;[5] we propose that this is also occurring for D_{par}. The PEP block is more entangled in this system, so N_B would correspond to N_{PEP} in eq 2. At 25 °C, N_e is 22 for PEP,[37] giving an N_B/N_e of 15.5. The amount of the PEP block in the pure PEP region, γ in eq 2, was estimated as follows. From the SAXS pattern in Figure 1 the d_{100} spacing is 31 nm. An estimate of the cylinder radius using this domain spacing and the volume fraction of the PDMS block is 8.5 nm. Helfand and Tagami derived a relationship for the interfacial width, a_∞[38]

$$a_\infty = 2\left(\frac{b_1^2 + b_2^2}{12\chi}\right)^{1/2} \tag{13}$$

where b_i is the statistical segment length of the monomer in block i. Broseta et al. added a correction for finite molecular weight[39]

$$a = a_\infty\left\{1 + \ln 2\left(\frac{1}{N_1\chi} + \frac{1}{N_2\chi}\right)\right\} \tag{14}$$

where N_i is the number of statistical segments of block i. At 25 °C the statistical segment lengths of PEP and PDMS are 0.57 and 0.79 nm, respectively.[37] Therefore, a is 1.4 nm, giving a γ of ca. 0.9. In Figure 7, the last three D_{par}/D_0 points have been fit to eq 2, using the N_B/N_e and γ given above, resulting in $\xi = 0.28$. Previously, a value $\xi = 0.17$ for block retraction in PEP−PEE lamellae was obtained,[5] in reasonable agreement with the result obtained here.

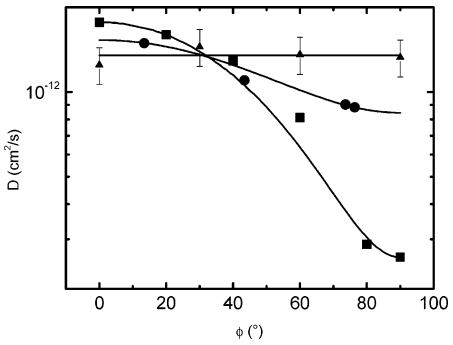

Figure 8. D vs ϕ for (■) $F_2 = 0.77$, (●) $F_2 = 0.26$, and (▲) $F_2 = 0.07$ at 80 °C.

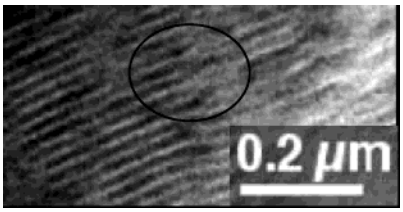

Figure 9. TEM image of a dislocation.

Contribution of Defects to the Measured D_{perp}. Figure 8 shows the diffusion coefficients obtained as a function of the sample orientation angle for $F_2 = 0.77$, 0.26, and 0.07 at 80 °C. The solid lines through the $F_2 = 0.77$ and 0.26 data are determined using eq 11 and the measured values of D_{perp} and D_{par} at each F_2. At $F_2 = 0.07$ $D_{par} \approx D_{perp}$ within the error of the measurement, and so the solid line is simply the average value of $D(\phi)$. Error bars corresponding to ±15%, a reasonable estimate of the typical uncertainty in the FRS diffusion measurement,[35,36] are also included for the $F_2 = 0.07$ data. There does not appear to be much dependence of D_{par} on F_2 within error of the measurement, but D_{perp} is strongly dependent on F_2. As F_2 increases, D_{perp} decreases from $D_{perp} \approx D_{par}$ at $F_2 = 0.07$. Therefore, we anticipate that D_{perp} at $F_2 = 1$ should be less than D_{perp} at $F_2 = 0.77$ and probably equal to D_s ($\approx 2 \times 10^{-14}$ cm^2/s at $T = 100$ °C).

From Figure 8 it is clear that as F_2 decreases, or the degree of alignment worsens, the apparent anisotropy of diffusion decreases; D_{perp} approaches D_{par}, and D_{par} is independent of F_2. Defects in the cylinder alignment could provide faster routes for diffusion and thereby increase the measured value of D_{perp}. Two types of defects to consider are misoriented cylinders and dislocations. In Figure 4 it can be observed that the cylinder axis tends to fluctuate about a preferred direction. Therefore, there will be regions of the sample that are locally misoriented with respect to the orientation angle. In these regions a chain will diffuse more or less rapidly, depending on whether the misorientation aligns the region more parallel or perpendicular than the overall orientation of the sample. Dislocations can also be observed in the sample by TEM. Figure 9 shows a TEM image; the PDMS cylinders are darker than the PI matrix. A dislocation is circled where two cylinders join together to form a fork. Depending on the degree of anisotropy it may take less time for a chain to diffuse around the fork rather than across the cylinders. Therefore, the dislocation could provide a faster route for diffusion, resulting in a larger apparent D_{perp}. By examining samples with different degrees of alignment, the effect of defects on diffusion can be explored.

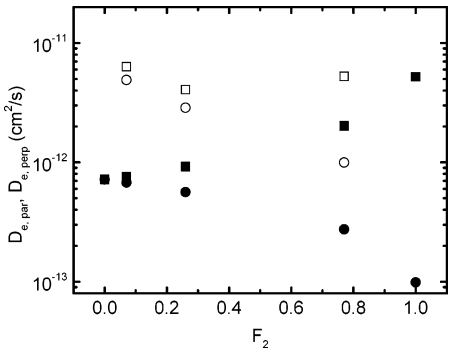

Figure 10. D_e vs F_2: (■) $D_{e,par}$, (●) $D_{e,perp}$. Also included are the experimental values of (□) D_{par} and (○) D_{perp}.

First, we consider the effect of misoriented cylinders on D_{par} and D_{perp}. If a chain is passing through a region that is misaligned by an angle ψ relative to the orientation angle ϕ, the observed diffusion coefficient of the chain in this region should be given by

$$D_\psi = D_{perp(0)} \sin^2(\phi - \psi) + D_{par(0)} \cos^2(\phi - \psi) \quad (15)$$

where $D_{perp(0)}$ and $D_{par(0)}$ are the hypothetical values of D_{perp} and D_{par} at $F_2 = 1$. The relative volume of regions misaligned at an angle ψ, V_ψ, can be estimated from the I vs θ plots in Figure 2, where

$$V_\psi \sim I(\theta - 90) \quad (16)$$

The distance a chain diffuses through this region, x_ψ, is proportional to $V_\psi^{1/3}$. The time it takes to diffuse through this region is x_ψ^2/D_ψ. Using the relation $D \sim x^2/t$, the effective diffusion coefficient at some orientation angle ϕ, $D_{e,\phi}$, is

$$D_{e,\phi} = \frac{\sum x_\psi^{\,2}}{\sum \frac{x_\psi^{\,2}}{D_\psi}} \quad (17)$$

Figure 10 shows a plot of $D_{e,par}$ and $D_{e,perp}$ calculated for each sample at 100 °C. For the calculation of D_ψ, D_s was used for $D_{perp(0)}$, and the average value of D_{par} with F_2 was used for $D_{par(0)}$ in eq 15. Also included on the plot are the experimentally measured values of D_{par} and D_{perp} vs F_2. In both the experiment and calculation, as F_2 decreases, the degree of anisotropy decreases. However, in the calculation, both $D_{e,par}$ and $D_{e,perp}$ approach an intermediate value between the D_{par} and D_{perp} at $F_2 = 1$, whereas in the experiment D_{par} is independent of F_2.

We conclude that the discrepancy between the calculated and observed behavior of D_{par} with F_2 arises because dislocations were not taken into account. To obtain a qualitative understanding of the effect of defects on D_{par} and D_{perp}, consider a perfectly aligned cylinder sample with dislocations approximated as struts between the cylinders, as shown in the cartoon in Figure 11. The total distance a chain has to diffuse is the grating spacing d, the average distance along a cylinder between dislocations is λ, and the domain spacing is L (determined from SAXS measurements to be ca. 40 nm). For a chain diffusing along the cylinders, the effective diffusion coefficient, $D_{e,par}$, is given by

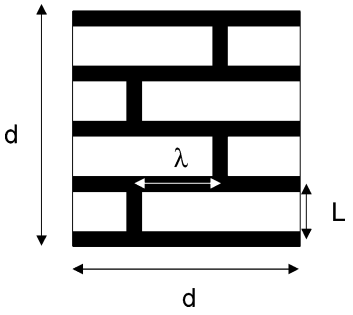

Figure 11. Cylinders with dislocations present. L is the domain spacing, λ is the average distance between defects, and d is the diffusion distance.

$$D_{e,par} = \frac{d^2}{t} \quad (18)$$

where t is the time it takes to diffuse along a cylinder plus the additional time to diffuse along any dislocation encountered:

$$t = \frac{d^2}{D_{par}} + \frac{\frac{d^2 L^2}{\lambda^2}}{D_{par}} \quad (19)$$

Therefore, $D_{e,\,par}$ is

$$D_{e,par} = \frac{D_{par}}{1 + \frac{L^2}{\lambda^2}} \quad (20)$$

For the perpendicular case it is assumed that parallel and perpendicular diffusion are independent processes. Therefore, the average diffusion time is given by

$$\frac{1}{t} = \frac{1}{t_{par}} + \frac{1}{t_{perp}} \quad (21)$$

where t_{par} and t_{perp} are the times required to diffuse either along or across cylinders for a distance d. The time for parallel diffusion is given in eq 22. It is the sum of the time to diffuse across the cylinders through dislocations plus the additional time to diffuse along cylinders from dislocation to dislocation.

$$t_{par} = \frac{d^2}{D_{par}} + \frac{\frac{d^2 \lambda^2}{L^2}}{D_{par}} \quad (22)$$

The time to diffuse perpendicular is

$$t_{perp} = \frac{d^2}{D_{perp}} \quad (23)$$

Therefore, the $D_{e,perp}$ is

$$D_{e,perp} = D_{perp} + \frac{D_{par}}{1 + \frac{\lambda^2}{L^2}} \quad (24)$$

D_s was used for D_{perp}, and the average value of D_{par} over

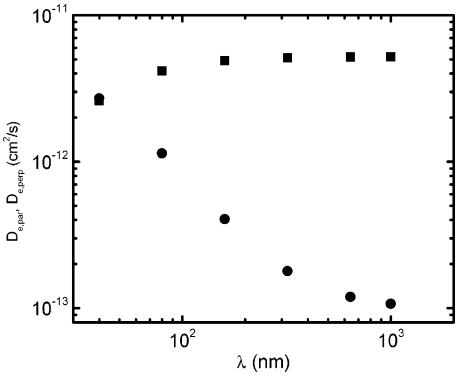

Figure 12. D_e vs λ: (■) $D_{e,par}$, (●) $D_{e,perp}$.

F_2 was used for D_{par} for these calculations. Figure 12 shows a plot of $D_{e,par}$ and $D_{e,perp}$ vs the dislocation spacing λ. The dislocations have a much greater effect on D_{perp} than D_{par}, with D_{par} only slowing down at high dislocation densities.

As the degree of alignment in the system decreases, the number of dislocations should increase. This will increase both D_{par} and D_{perp} compared to the calculated $D_{e,par}$ and $D_{e,perp}$ in Figure 10. For parallel diffusion defects can speed up the diffusion in misaligned regions if they provide a lower resistance path. This makes D_{par} less sensitive to the degree of alignment than D_{perp}. There could be some subtle variation in D_{par} with the degree of alignment depending on the relationship between F_2 and the defect density, although one could not be discerned here. D_{perp} is highly dependent on both the degree of alignment and the defect density. The defect density needed to increase $D_{e,perp}$ to the measured D_{perp} in Figure 10 can be estimated as follows. To determine $D_{e,perp}$ due to misaligned cylinders, eq 15 was used to estimate D at different angles of orientation of the cylinders. In this equation, $D_{perp(0)} = D_s$ was assumed, but $D_{perp(0)}$ must be greater than D_s due to dislocations speeding up the diffusion. The effective diffusion coefficient due to dislocations is the value of $D_{perp(0)}$ needed for $D_{e,perp}$ determined in eq 17 to equal the measured value of D_{perp}. Then the distance between dislocations can be determined from $D_{perp(0)}$ using the data in Figure 12. For $F_2 = 0.77$, 0.26, and 0.07 the λ values are 120, 55, and 16 nm, respectively. These values follow the expected trend; the defect density increases as the degree of alignment in the samples decreases. However, these defect densities are larger than expected. One possible contribution is that $D_{par(0)}$ is in fact greater than the average value of D_{par}. If $D_{par(0)}$ is larger, this would have two effects. It would make dislocations more effective at accelerating diffusion, and the $D_{e,perp}$ curve in Figure 12 would shift to the right toward higher λ. Second, it would decrease the value of $D_{perp(0)}$ needed for $D_{e,perp}$ calculated in eq 17 to equal D_{perp} measured and thereby also increase λ. However, this analysis of the role of defects is certainly oversimplified, so quantitative agreement should not be expected.

Summary

Self-diffusion has been measured in ordered PEP−PDMS cylinders over a range of macroscopic alignments. In well-aligned cylinders there is a large anisotropy of diffusion with $D_{par} > D_{perp}$. This anisotropy arises from the different mechanisms of diffusion for D_{par} and D_{perp}. D_{perp} followed a hindered diffusion mechanism, with a barrier that is exponentially dependent on χN_A. In contrast, D_{par} crosses over to a block retraction mechanism where the diffusion barrier is exponentially dependent on $N_{PEP}/N_{e,PEP}$ but independent of χ. Additionally, D_{perp} was found to be strongly dependent on the degree of alignment, while D_{par} was not. Both misaligned cylinders and dislocations can act to accelerate the diffusion in the perpendicular orientation, resulting in a larger apparent D_{perp}. Therefore, it is very difficult to measure D_{perp} when there is a high degree of anisotropy, unless the sample is almost perfectly oriented.

Acknowledgment. This work was supported by the National Science Foundation, through Award DMR-9901087, and also by the Graduate School of the University of Minnesota, through a Doctoral Dissertation Fellowship (K.A.C.). Special thanks is given to Zhibo Li for performing the TEM experiments.

References and Notes

(1) Fleischer, G.; Rittig, F.; Štepánek, P.; Almdal, K.; Papadakis, C. M. *Macromolecules* **1999**, *32*, 1956.
(2) Dalvi, M. C.; Eastman, C. E.; Lodge, T. P. *Phys. Rev. Lett.* **1993**, *71*, 2591.
(3) Dalvi, M. C.; Lodge, T. P. *Macromolecules* **1994**, *27*, 3487.
(4) Kannan, R. M. *J. Chem. Phys.* **1998**, *108*, 4634.
(5) Lodge, T. P.; Dalvi, M. C. *Phys. Rev. Lett.* **1995**, *75*, 657.
(6) Lodge, T. P.; Hamersky, M. W.; Milhaupt, J. M.; Kannan, R. M.; Dalvi, M. C.; Eastman, C. E. *Macromol. Symp.* **1997**, *121*, 219.
(7) Rittig, F.; Kärger, J.; Papadakis, C. M.; Fleischer, G.; Štepánek, P.; Almdal, K. *Phys. Chem. Chem. Phys.* **1999**, *1*, 3923.
(8) Shull, K. R.; Kramer, E. J.; Bates, F. S.; Rosedale, J. H. *Macromolecules* **1991**, *24*, 1383.
(9) Rittig, F.; Fleischer, G.; Kärger, J.; Papadakis, C. M.; Almdal, K.; Štepánek, P. *Macromolecules* **1999**, *32*, 5872.
(10) Hamersky, M. W.; Tirrell, M.; Lodge, T. P. *Langmuir* **1998**, *14*, 6974.
(11) Hamersky, M. W.; Hillmyer, M. A.; Tirrell, M.; Bates, F. S.; Lodge, T. P.; von Meerwall, E. D. *Macromolecules* **1998**, *31*, 5363.
(12) Papadakis, C. M.; Almdal, K.; Mortensen, K.; Rittig, F.; Štepanek, P. *Macromol. Symp.* **2000**, *162*, 275.
(13) Rittig, F.; Kärger, J.; Papadakis, C. M.; Fleischer, G.; Almdal, K.; Tepánek, P. *Macromolecules* **2001**, *34*, 868.
(14) Cavicchi, K. A.; Lodge, T. P. *Macromolecules* **2003**, *36*, 7158.
(15) Yokoyama, H.; Kramer, E. J. *Macromolecules* **1998**, *31*, 7871.
(16) Barrat, J.-L.; Fredrickson, G. H. *Macromolecules* **1991**, *24*, 6378.
(17) Yokoyama, H.; Kramer, E. J.; Fredrickson, G. H. *Macromolecules* **2000**, *33*, 2249.
(18) Eastman, C. E.; Lodge, T. P. *Macromolecules* **1994**, *27*, 5591.
(19) Fredrickson, G. H.; Milner, S. T. *Mater. Res. Soc. Symp. Proc.* **1990**, *177*, 169.
(20) Rubinstein, M.; Obukhov, S. P. *Macromolecules* **1993**, *26*, 1740.
(21) de Gennes, P. G. *J. Phys. (Paris)* **1975**, *36*, 1199.
(22) de Gennes, P. G. *J. Chem. Phys.* **1971**, *55*, 572.
(23) Dalvi, M. C.; Lodge, T. P. *Macromolecules* **1993**, *26*, 859.
(24) Vigild, M. E. Riso Natl. Lab., Roskilde, Denmark, 1997.
(25) Fredrickson, G. H.; Helfand, E. *J. Chem. Phys.* **1987**, *87*, 697.
(26) Lodge, T.; Chapman, B. *Trends Polym. Sci.* **1997**, *5*, 122.
(27) Sakurai, S.; Aida, S.; Okamoto, S.; Ono, T.; Imaizumi, K.; Nomura, S. *Macromolecules* **2001**, *34*, 3672.
(28) Zalusky, A. S.; Olayo-Valles, R.; Wolf, J. H.; Hillmyer, M. A. *J. Am. Chem. Soc.* **2002**, *124*, 12761.
(29) Ehlich, D.; Takenaka, M.; Hashimoto, T. *Macromolecules* **1993**, *26*, 492.

(30) de Gennes, P. G. *The Physics of Liquid Crystals*; Oxford University Press: New York, 1993.
(31) Thurston, G. B. *Appl. Opt.* **1964**, *3*, 755.
(32) Lodge, T. P.; Fredrickson, G. H. *Macromolecules* **1992**, *25*, 5643.
(33) Milhaupt, J. PhD Thesis, University of Minnesota, Minneapolis, MN, 2000.
(34) Shewmon, P. *Diffusion in Solids*, 2nd ed.; The Minerals, Metals & Materials Society: Warrendale, PA, 1989.
(35) Dalvi, M. C. PhD Thesis, University of Minnesota, Minneapolis, MN, 1994.
(36) Hamersky, M. PhD Thesis, University of Minnesota, Minneapolis, MN, 1997.
(37) Fetters, L. J.; Lohse, D. J.; Richter, D.; Witten, T. A.; Zirkel, A. *Macromolecules* **1994**, *27*, 4639.
(38) Helfand, E.; Tagami, Y. *J. Polym. Sci., Part C: Polym. Lett.* **1971**, *9*, 741.
(39) Broseta, D.; Fredrickson, G. H.; Helfand, E.; Leibler, L. *Macromolecules* **1990**, *23*, 132.

MA0495339